Perturbative approach to the capacitive interaction between a sensor quantum dot and a charge qubit

S. Mojtaba Tabatabaei*
Faculty of Physics, Shahid Beheshti University, Tehran, Iran
(Received 19 October 2016; revised manuscript received 19 February 2017; published 10 April 2017)

We consider the capacitive interaction between a charge qubit and a sensor quantum dot (SQD) perturbatively to the second order of their coupling constant at zero temperature by utilizing the method of nonequilibrium Green's functions together with infinite-U Lacroix approximation and employing Majorana fermion representation for qubit isospin operators. The effect of back-actions on dynamics of the system is taken into account by calculating the self-energies and the Green's functions in a self-consistent manner. To demonstrate the applicability of the method, we investigate relevant physical quantities of the system at zero and finite bias voltages. In the regime of weak SQD-qubit coupling, we find a linear relation between the stationary-state expectation values of the third component of the qubit isospin vector, $\langle\tau_3\rangle$, and the differential conductance of the SQD. Furthermore, our numerical results predict that the effect of SQD-qubit coupling on differential conductance of the SQD should be maximized at zero bias voltage. Moreover, we obtain an analytical expression to describe the behavior of the differential conductance of the SQD with respect to the qubit parameters. Our results at zero bias voltage are consistent with the results of numerical renormalization group method.

DOI: 10.1103/PhysRevB.95.155113

I. INTRODUCTION

Typically, the state of a solid-state qubit could be indirectly extracted by measuring the conductance of a current-carrying electrometer which is capacitively coupled to the qubit. This detector, which could be realized in the experiment by a quantum point contact (QPC) [1–8] or a single-electron transistor (SET) [9–16], provides us with measurements of the charge fluctuations of qubit. The usage of SETs is, however, more advantageous to the QPCs because of their much greater sensitivity to the charge fluctuations [16]. In practice, the coupling of the sensor quantum dot (SQD) of the SET with qubit is made so weak in order to reduce the effect of measurements on the qubit state. However, no matter how weak it is, the system inevitably suffers from coupling effects, which results in a coherent backaction on the qubit dynamics and renormalization of the system energy levels [17,18].

Using SET as a qubit detector has been the subject of several theoretical studies [19–31]. Much work has been devoted to investigating the time-dependent dynamics of the reduced density matrix of the system taking into account the leading-order tunneling processes in the SET and ignoring the backaction of qubit and SET on each other [21–24]. The problem of considering the effects of backactions on the SET-qubit system in the presence of external bias was also studied in Refs. [25–31]. Recently, Hell *et al.* [30,31] studied the coherent backaction of the measurements on the SET-qubit system in the presence of finite bias by deriving Markovian kinetic equations for the system taking into account next-to-leading-order corrections in the tunneling processes of the SET and the effects of the energy levels's renormalization of the system.

Here, we consider the application of the method of nonequilibrium Green's functions for describing the nonequilibrium dynamics of the SET-qubit system. We calculate the steady-state nonequilibrium Green's functions of the system at zero temperature using second-order self-energies of the capacitive coupling between a SQD and a qubit. Due to the lack of applicability of Wick's theorem for Pauli operators, we utilize the Majorana fermion representation [32–34] for the qubit isospin operators by which a systematic diagrammatic perturbative expansion of the system's Green's functions become possible. In order to take into account strong electron-electron interaction on the SQD, which is necessary to keep it in the Coulomb blockade regime, we employ the infinite-U Lacroix approximation [35] to calculate the bare Green's functions of the SQD. The backaction effects on the average occupations of the SQD and the qubit are accounted for by calculating the self-energies and the Green's functions self-consistently. Using the calculated interacting Green's functions of the system, we investigate the density of states of the SQD and the steady-state expectation value of the third component of the isospin operator of the qubit, $\langle\tau_3\rangle$. Furthermore, we determine the differential conductance of the SQD at zero and finite bias voltages and show that there is a linear relation between the SQD's differential conductance and the steady-state expectation value $\langle\tau_3\rangle$. We check the accuracy of our results at zero bias by comparing them with the results obtained from the numerical renormalization group (NRG) method [36].

Our approach differs basically from density-matrix-based approaches [37]. In the latter, it is the coupling of a SQD with electrodes which is considered perturbatively for calculating the reduced density matrix of the subsystem. Hence, the possible partial coherences between different charge states of the SQD during tunneling processes are ignored trivially. Instead, in our approach, the parameter that is used for perturbatively obtaining the Green's functions of the system is the capacitive coupling between the SQD and the qubit while the effects of coupling between the SQD and the metallic electrodes are incorporated nonperturbatively into the Green's functions of the SQD, which retains the possible partial coherences of the SQD's charge states.

*s.m.taba90@gmail.com

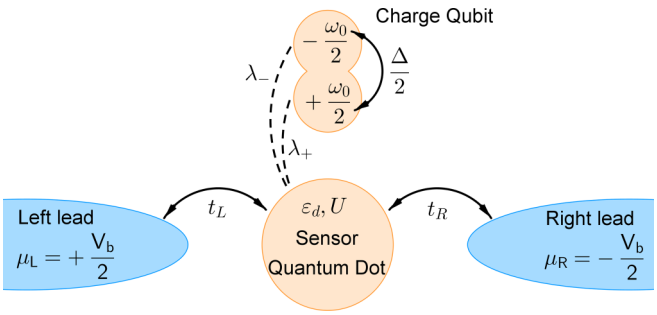

FIG. 1. Schematic representation of the model system. The sensor quantum dot, characterized with gate voltage ε_d and on-site interaction U, coupled to two metallic leads and simultaneously interacts capacitively with one double quantum dot through interaction constants λ_+ and λ_-. The on-site energies of DQD are $\pm\omega_0/2$ and the tunneling energy between its dots is specified by $\Delta/2$.

The paper is organized as follows. In Sec. II A, the model Hamiltonian is presented. Then in Sec. II B, we present the derivation of nonequilibrium Green's functions of the SQD-qubit system. After that, in Sec. II C, we give some expressions for relating different physical quantities of the system with the Green's functions. We present our numerical results in Sec. III. Then, in Sec. IV, we give a summary of our work and some concluding remarks related to it.

II. THEORETICAL FORMALISM

A. Model Hamiltonian

Our model system, as depicted in Fig. 1, consists of a SQD in a Coulomb-blockade regime tunnel coupled to two metallic electrodes while simultaneously interacting capacitively with a charge qubit which is modeled by a double quantum dot (DQD). The total Hamiltonian of the system can be written as

$$\mathcal{H} = \mathcal{H}_{\rm SET} + \mathcal{H}_{\rm DQD} + \mathcal{H}_I. \tag{1}$$

The first term is the Hamiltonian of SET, which is given by

$$\begin{aligned}\mathcal{H}_{\rm SET} = &\sum_{\nu}\varepsilon_d\, c^\dagger_{d,\nu}c_{d,\nu} + U n_{d,\uparrow}n_{d,\downarrow}\\ &+\sum_{k,\alpha,\nu}(\varepsilon_k+\mu_\alpha)\, c^\dagger_{k,\alpha,\nu}c_{k,\alpha,\nu}\\ &+t_\alpha\,(c^\dagger_{k,\alpha,\nu}c_{d,\nu}+\text{H.c.}),\end{aligned} \tag{2}$$

where the operator $c^\dagger_{d,\nu}$ ($c_{d,\nu}$) creates (annihilates) an electron with spin $\nu=\uparrow,\downarrow$ in the SQD, $n_{d,\nu}=c^\dagger_{d,\nu}c_{d,\nu}$ is the spin-dependent electron occupation operator of SQD, ε_d is the applied gate voltage, and U is the on-site electron-electron interaction energy in SQD. Similarly, the operator $c^\dagger_{k,\alpha,\nu}$ ($c_{k,\alpha,\nu}$) is the corresponding operator for electron creation (annihilation) with energy ε_k in the left and right leads ($\alpha = L,R$), each of which is treated as half-filled quasi-one-dimensional normal metals with chemical potentials μ_L and μ_R, respectively. The coupling of the SQD with each lead is assumed to be energy and spin independent and characterized by a hybridization constant, $t_{L,R}$.

The second term in Eq. (1) is the Hamiltonian of the charge qubit, which is modeled as a double quantum dot [38] containing only one electron, with on-site energies $\pm\frac{\omega_0}{2}$ and hybridization energy $\frac{\Delta}{2}$. Representing the state of the electron on each of the DQD's dots by $|+\rangle$ and $|-\rangle$, in terms of isospin operators (τ_1,τ_2,τ_3) the DQD's Hamiltonian takes the form

$$\mathcal{H}_{\rm DQD} = -\frac{\omega_0}{2}\tau_3 + \frac{\Delta}{2}\tau_1. \tag{3}$$

The last term in Eq. (1) is the capacitive interaction between the SQD and the DQD, which is $2n_d(\lambda_+ n_+ + \lambda_- n_-)$, where $\lambda_{+,-}$ is an interaction constant and $n_d = n_{d,\uparrow}+n_{d,\downarrow}$ is the total electron number operator of the SQD. Furthermore, $n_{+,-}$ represents the occupation number operator of each dot of the DQD. By using the relation $n_\pm = \frac{1}{2}(1\pm\tau_3)$ and an appropriate renormalization of ε_d, the interaction can be expressed as $\lambda n_d\tau_3$, where $\lambda \equiv \lambda_+ - \lambda_-$. In addition, for later convenience, we explicitly take into account the mean-field backaction effects by adding and subtracting the operator $A = \lambda(\langle n_d\rangle\tau_3 + \langle\tau_3\rangle n_d)$ to the total Hamiltonian. This modifies the on-site energies of the SQD and DQD to $\tilde{\varepsilon}_d = \varepsilon_d + \lambda\langle\tau_3\rangle$ and $\tilde{\omega}_0 = \omega_0 - 2\lambda\langle n_d\rangle$, respectively, and then the interaction term of the Hamiltonian becomes

$$\mathcal{H}_I = \lambda(n_d - \langle n_d\rangle)(\tau_3 - \langle\tau_3\rangle). \tag{4}$$

In order to use perturbation theory, we need to express the isospin operators in terms of Majorana fermion operators by [34]

$$\tau_a = -i\epsilon_{abc}\eta_b\eta_c \tag{5}$$

for $a,b,c = 1,2,3$, where ϵ_{abc} is the Levi-Civita antisymmetric tensor and (η_1,η_2,η_3) are three Majorana fermion operators satisfying usual fermionic equal-time anticommutation relation $\{\eta_a,\eta^\dagger_b\} = \delta_{a,b}$, with $\eta^\dagger_a = \eta_a$.

B. Nonequilibrium Green's functions

The nonequilibrium Green's function method is a usual choice to study out-of-equilibrium systems [39]. We will treat $\mathcal{H}_{\rm SQD}+\mathcal{H}_{\rm DQD}$ and $\mathcal{H}_I$ as the noninteracting and interaction parts of Hamiltonians, respectively. A complete description of the nonequilibrium steady state of a system requires the knowledge of four Green's functions; we choose the retarded, advanced, lesser, and greater, defined, respectively, for the noninteracting system as

$$g^R_{s,mn}(t,t') = -i\theta(t-t')\langle\{\Psi_{s,m}(t),\Psi^\dagger_{s,n}(t')\}\rangle_0, \tag{6a}$$

$$g^A_{s,mn}(t,t') = i\theta(t'-t)\langle\{\Psi_{s,m}(t),\Psi^\dagger_{s,n}(t')\}\rangle_0, \tag{6b}$$

$$g^<_{s,mn}(t,t') = i\langle\Psi^\dagger_{s,n}(t')\Psi_{s,m}(t)\rangle_0, \tag{6c}$$

and

$$g^>_{s,mn}(t,t') = -i\langle\Psi_{s,m}(t)\Psi^\dagger_{s,n}(t')\rangle_0, \tag{6d}$$

where $s = d,\eta$ determines the corresponding subsystem for which the Green's functions are defined and m,n represent degrees of freedom for the corresponding subsystem, that is, in the case of the SQD, $\Psi_{d,m} = c_{d,m}$, with $m=\uparrow,\downarrow$ while for the DQD, $\Psi_{\eta,m} = \eta_m$, with $m = 1,2,3$. In addition, $\langle\cdots\rangle_0$ is the expectation value with respect to the ground state of

$\mathcal{H}_{\rm SQD}+\mathcal{H}_{\rm DQD}$ at zero temperature. In the sequel, the term interacting/noninteracting is used to account for the interaction between the SQD and the DQD and not for the on-site interactions in the SQD. Also, we will present noninteracting and interacting Green's functions as g and $\mathcal{G}$, respectively. Furthermore, because our Hamiltonian does not explicitly depend on time, the Green's functions become functions of time differences only and it is therefore more preferable to express them in the frequency space by Fourier transformation.

The inclusion of interactions is performed by using the Dyson equation through which the exact retarded Green's function of the system could be determined by

$$\mathcal{G}^R(\omega)=[\mathcal{G}^A(\omega)]^\dagger=g^R(\omega)+g^R(\omega)\Sigma^R(\omega)\mathcal{G}^R(\omega), \tag{7}$$

while the exact lesser Green's function has the form

$$\mathcal{G}^<(\omega)=\mathcal{G}^R(\omega)\Sigma^<(\omega)\mathcal{G}^A(\omega), \tag{8}$$

where $\Sigma^{R,<}(\omega)$ stands for the total proper retarded and lesser self-energies of the system. The greater Green's function is then obtained using $\mathcal{G}^>(\omega)=\mathcal{G}^A(\omega)-\mathcal{G}^R(\omega)+\mathcal{G}^<(\omega)$.

1. Green's functions of SQD

In order to maximize the sensitivity of the SET, the energy level of the SQD should be tuned to the flank of the Coulomb blockade peak. In this regime, the cotunneling processes between the SQD and the leads become dominant and the conventional sequential tunneling approximations ceased to be applicable for describing the state of the SQD. Therefore, we use the infinite-U Lacroix approximation, which is believed to consider cotunnelings in the Coulomb-blockade regime, in order to obtain the Green's functions of the SQD, g_d^R, which will be used later as building blocks of the self-energies. By using Eq. (17) of Ref. [40], we obtain the Fourier transform of the diagonal elements of the SQD's retarded Green's function matrix as

$$g^R_{d,\nu\nu}(\omega)=\frac{1-\langle n_{d,\bar\nu}\rangle+P_\nu(\omega)}{\omega+i\delta-\tilde\varepsilon_d+i(\Gamma_L+\Gamma_R)-Q_\nu(\omega)}, \tag{9}$$

where δ is an infinitesimal positive constant and $\Gamma_{L,R}\equiv\pi|t_{L,R}|^2\rho_0$ is the broadening of the SQD's energy level due to its coupling to the leads in the standard wideband limit in which the density of states of the leads, ρ_0, is assumed to be independent of energy. Furthermore,

$$P_\nu(\omega)=\sum_{\alpha=L,R}\frac{\Gamma_\alpha}{\pi}\int d\omega_1\frac{g^A_{d,\nu\nu}(\omega_1)f_\alpha(\omega_1)}{\omega+i\delta-\omega_1} \tag{10a}$$

and

$$Q_\nu(\omega)=\sum_{\alpha=L,R}\frac{\Gamma_\alpha}{\pi}\int d\omega_1\frac{\big[1+i\Gamma g^A_{d,\nu\nu}(\omega_1)\big]f_\alpha(\omega_1)}{\omega+i\delta-\omega_1}, \tag{10b}$$

where $f_{L,R}(\omega)=\theta(\mu_{L,R}-\omega)$ and $\theta(\cdots)$ is the standard Heaviside-θ function. For the noninteracting lesser Green's function of the SQD, $g_d^<(\omega)$, we have

$$g_d^<(\omega)=g_d^R(\omega)\Sigma_d^{({\rm U})<}(\omega)g_d^A(\omega), \tag{11}$$

where $\Sigma_d^{({\rm U})<}$ is calculated using the ansatz [41]

$$\Sigma_d^{({\rm U})<}(\omega)=\big\{\big[g_d^R(\omega)\big]^{-1}-\big[g_d^A(\omega)\big]^{-1}\big\}\sum_{\alpha=L,R}\frac{\Gamma_\alpha f_\alpha(\omega)}{\Gamma}. \tag{12}$$

Using the second-order self-energies of the SQD, which are given in Appendix A, the interacting retarded and lesser Green's functions of the SQD can be obtained as

$$\mathcal{G}_d^R(\omega)=g_d^R(\omega)+g_d^R(\omega)\Sigma_d^{(2nd)R}(\omega)\mathcal{G}_d^R(\omega) \tag{13}$$

and

$$\mathcal{G}_d^<(\omega)=\mathcal{G}_d^R(\omega)\big[\Sigma_d^{({\rm U})<}(\omega)+\Sigma_d^{(2nd)<}(\omega)\big]\mathcal{G}_d^A(\omega). \tag{14}$$

2. Green's functions of DQD

Using the method of equations of motion, the Fourier transform of the noninteracting retarded Green's functions of the DQD, g_η^R, can be computed from a set of nine equations,

$$\begin{aligned}(\omega+i\delta)g^R_{\eta,mn}=\delta_{mn}&+\delta_{1m}\tilde\omega_0 g^R_{\eta,2n}\\&-\delta_{2m}\big(\tilde\omega_0 g^R_{\eta,1n}+\Delta g^R_{\eta,3n}\big)+\delta_{3m}\Delta g^R_{\eta,2n},\end{aligned} \tag{15}$$

where $m,n=1,2,3$ and δ_{mn} is the Kronecker-delta. The solution of the above equations in matrix form is

$$g^R_\eta(\omega)=\begin{pmatrix}\omega+i\delta & -i\tilde\omega_0 & 0\\ i\tilde\omega_0 & \omega+i\delta & i\Delta\\ 0 & -i\Delta & \omega+i\delta\end{pmatrix}^{-1}. \tag{16}$$

Accordingly, the noninteracting lesser Green's function of the DQD is

$$g_\eta^<(\omega)=-2i{\rm Im}\big[g_\eta^R(\omega)\big]f(\omega), \tag{17}$$

where $f(\omega)=\theta(-\omega)$.

Now we can use the self-energies of the DQD, which are derived in Appendix A, to calculate the interacting retarded and lesser Green's functions of the DQD:

$$\mathcal{G}_\eta^R(\omega)=g_\eta^R(\omega)+g_\eta^R(\omega)\Sigma_\eta^{(2nd)R}(\omega)\mathcal{G}_\eta^R(\omega) \tag{18}$$

and

$$\mathcal{G}_\eta^<(\omega)=\mathcal{G}_\eta^R(\omega)\Sigma_\eta^{(2nd)<}(\omega)\mathcal{G}_\eta^A(\omega). \tag{19}$$

C. Physical quantities

By using the definition of the lesser Green's function [Eq. (6c)], the expectation values of n_d and τ_3 are

$$\langle n_d\rangle=-\frac{i}{2\pi}\int d\omega{\rm Tr}[\mathcal{G}_d^<(\omega)] \tag{20}$$

and

$$\langle\tau_3\rangle=-2\int\frac{d\omega}{2\pi}\mathcal{G}^<_{\eta,12}(\omega). \tag{21}$$

Furthermore, the average electric current through the SQD in the steady state could be calculated by

$$I=-\frac{e}{\hbar}\int\frac{d\omega}{2\pi}\Gamma_L{\rm Tr}\big\{{\rm Im}\big[\mathcal{G}_d^<(\omega)+2\mathcal{G}_d^R(\omega)f_L(\omega)\big]\big\}, \tag{22}$$

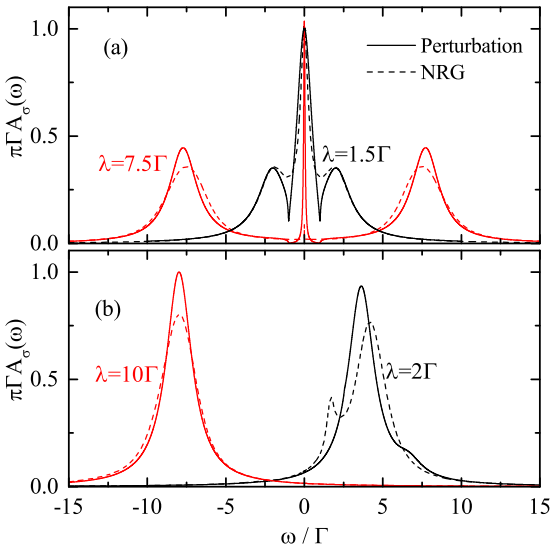

FIG. 2. Comparison of single-spin spectral densities of the SQD calculated by the perturbation method (solid lines) and with the NRG method (dashed lines), with $U = 0$, $\Delta = \Gamma$, and $V_b = 0$. For (a), $\varepsilon_d = 0$, $2\lambda = \omega_0 = 3\Gamma, 15\Gamma$; for (b), $\varepsilon_d = 2\Gamma$, $\lambda = \frac{2}{3}\omega_0 = 2\Gamma, 10\Gamma$.

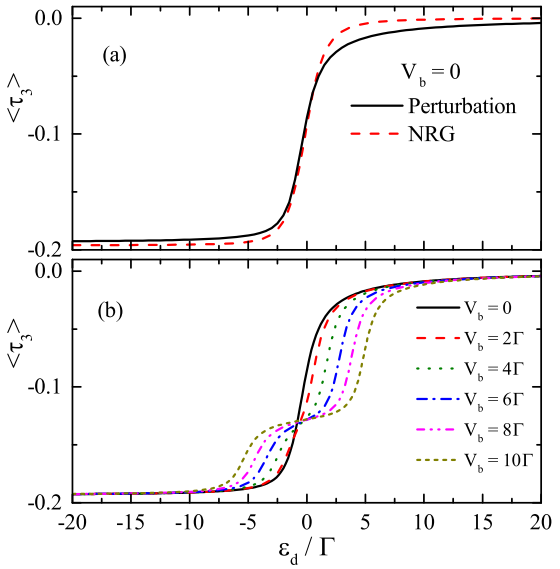

FIG. 3. Average values of τ_3 with respect to ε_d for $\omega_0 = 0$, $\Delta = 0.1\Gamma$, and $\lambda = 0.01\Gamma$ at (a) zero bias and (b) finite bias.

from which we can obtain the differential conductance of the SQD through $G = \frac{dI}{dV_b}$.

For future reference, we also define the "signal differential conductance" of the SQD [16,42], which is defined as the difference of the SQD's conductance in the presence of the DQD and in the absence of it. It is represented by

$$\delta G = G_{\lambda \neq 0} - G_{\lambda = 0}. \tag{23}$$

III. RESULTS AND DISCUSSIONS

Here we present our numerical results for zero and finite bias voltages. We calculate self-consistently the self-energies and the Green's functions of the system (see Appendix B for a brief outline of our self-consistent calculations method). The calculations are performed at zero temperature $T = 0$, and $\Gamma = \Gamma_L + \Gamma_R$ is taken as unit of energy. Furthermore, we take $\hbar = e = c = 1$. The finite bias is established by considering a symmetric bias voltage between two metallic leads as $\mu_L = -\mu_R = \frac{V_b}{2}$. In zero bias, we check our results by comparing them with NRG results which are obtained by utilizing the "NRG LJUBLJANA" [43] package. In all NRG calculations we set the logarithmic discretization parameter to $\Lambda = 2$ and kept up to 1000 states for each iteration diagonalizations.

A. Spectral densities and average occupation values

In Fig. 2, we compare the single-spin QD's local density of states, $A_\sigma(\omega) = -\frac{1}{\pi}\mathrm{Im}[\mathcal{G}^R_{d,\sigma\sigma}(\omega)]$, obtained from our perturbative approach and the NRG method. For simplicity, we take $U = 0$ and fix the value of Δ to Γ, while we set different values to the λ, ω_0, and ε_d. In Fig. 2(a), for the particle-hole symmetric case, $\varepsilon_d = 0$ and $2\lambda = \omega_0$, we see good agreement between perturbative results and NRG except the rate of narrowing of the central peak and the height of the broad sidebands in the case of large λs. In Fig. 2(b), we show density of states for two particle-hole asymmetric configurations. The position of the broad peaks are in good agreement with NRG, whereas their heights differ with it.

Next we consider the presence of large on-site interactions on the SQD (infinite U) and focus on the weak-coupling parameter regime where the condition $\lambda \ll \Delta \ll \Gamma$ is satisfied. We set the energy difference between the two dots of DQD to zero, $\omega_0 = 0$, and study the average occupation values of qubit for different gate voltages of the SQD in Fig. 3. Generally, it is expected that the value of $\langle\tau_3\rangle$ becomes zero, i.e., ($\langle n_\pm\rangle = \frac{1}{2}$), when there is no electron in the SQD and, by the presence of an electron on the SQD, the $\langle\tau_3\rangle$ acquires a negative value to recover itself in the new potential energy of the qubit. In Fig. 3(a) the average values $\langle\tau_3\rangle$, obtained separately by our self-consistent method and the NRG, are depicted as a function of ε_d for fixed $\Delta = 0.1\Gamma$ and $\lambda = 0.01\Gamma$ when there is no applied bias. We see almost good agreement with the NRG. In the presence of finite bias voltages, as is shown in Fig. 3(b), we see that by increasing bias voltages, a step starts to appear in the average values $\langle\tau_3\rangle$ in the range $-\frac{V_b}{2} < \varepsilon_d < \frac{V_b}{2}$, where the SQD has merely the same probability for being occupied or unoccupied and therefore $\langle\tau_3\rangle$ acquires a midvalue between zero and its minimum value.

B. Differential conductance

For a SQD with $U = 0$ and in the weak-coupling parameter regime, we can find an analytical expression for δG which clearly shows linear relation with $\langle\tau_3\rangle$ (see Appendix C for a derivation). Our numerical results for this case are also giving this linear relation perfectly (not shown here). On the other hand, in the case of a SQD with infinite U, due to the requirement of self-consistent calculations, obtaining an analytical expression for δG is seems to be impossible, at least in the context of the nonequilibrium Green's functions formalism. Thus, in order to check the linear dependence of δG on $\langle\tau_3\rangle$, we concentrate only on numerical results. In Fig. 4, our numerical results for δG as a function of $\langle\tau_3\rangle$

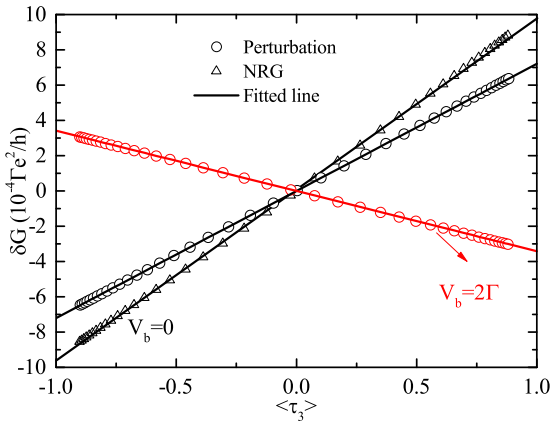

FIG. 4. Plot of δG calculated by the perturbative method (circles) and the NRG method (triangles) with respect to $\langle\tau_3\rangle$ in zero bias (black) and finite bias (red) voltages with $\varepsilon_d = 0$, $\Delta = 0.1\Gamma$, $\lambda = 0.01\Gamma$.

at zero and finite bias voltages are shown. We see that our perturbative results (circles) are fitted entirely to a line which clearly demonstrates the linear dependence of δG on $\langle\tau_3\rangle$. An important feature in Fig. 4 is the linear dependence of NRG results (triangles) for δG with respect to $\langle\tau_3\rangle$ at zero bias. This NRG linear dependence could be thought of as a complementary confirmation for our observations although its line slope differs slightly from that of our perturbative results.

In Fig. 5, the dependence of δG on the various parameters of the system is shown. In Fig. 5(a), δG is depicted as a function of ε_d for different bias voltages while the values of Δ, λ, and ω_0 are kept fixed. We see that the curves of δG go from an infinitesimal positive value for $\varepsilon_d \ll 0$ to an infinitesimal negative value for $\varepsilon_d \gg 0$, while for intermediate values of ε_d, they show some oscillations. By increasing the value of V_b, the oscillations change from a "one-peak, one-dip" to a "two-peak, two-dip" shape, and also the positions of the peaks/dips are pushed from the center. Another remarkable feature is the decreasing of the amplitude of the δG curves by increasing the bias voltage. In other words, we predict that the amplitudes for oscillations of signal differential conductances are maximized at zero bias voltage. Next, we study the impact of changing Δ on δG in Fig. 5(b). We see that increasing Δ has a reduction effect on δG and decreases the amplitude of the differential signal conductances. The other parameter of the system which should have some effects on δG is the energy difference between the two quantum dots of the charge qubit (ω_0). In Fig. 5(c), we investigate the impact of different values of ω_0 on δG. We see that the positions ε_d of the peaks are almost intact; however, the amplitudes of the δG curves change considerably by changing ω_0.

In order to describe the aforementioned dependence of δG on Δ and ω_0, we focus on the peaks which are specified in Figs. 5(b) and 5(c) by vertical dashed lines and plot the calculated values of δG with respect to the ω_0 and Δ, respectively, in Figs. 6(a) and 6(b). Surprisingly, we see that both numerical data points in Figs. 6(a) and 6(b) are fitted perfectly to the function $f[\omega_0, \Delta] = c(\omega_0 - a)/\sqrt{(\omega_0 - a)^2 + \Delta^2}$. We could intuitively interpret this behavior by the fact that the ground-state expectation value of τ_3 for an isolated charge

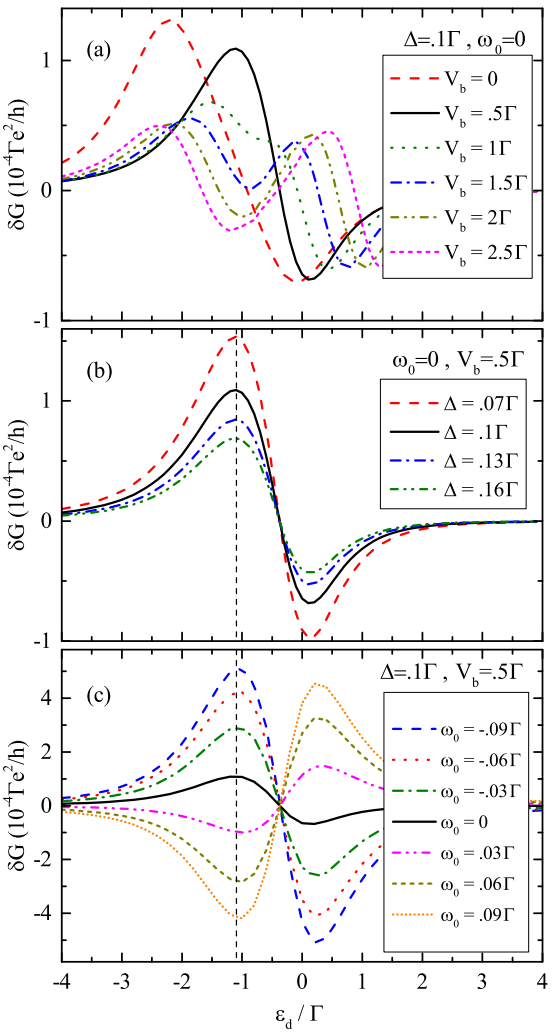

FIG. 5. Differential signal conductance of the SQD as a function of ε_d for $\lambda = 0.01\Gamma$ with respect to (a) V_b, (b) Δ, and (c) ω_0.

qubit, with the same configuration as in our model system, is equal to $\langle\tau_3\rangle_{\text{isolated}} = -\omega_0/\sqrt{\omega_0^2 + \Delta^2}$. As a result, the above functional form for δG would be expected to describe correctly the linear relation of δG with the ground-state expectation value of τ_3 of a charge qubit which is capacitively coupled to the SQD.

From an experimental point of view, the above relation for δG suggests a possible indirect measurement of the stationary-state value of $\langle\tau_3\rangle$ by measuring δG. By setting the value of ω_0 to a very large value ($\omega_0 \to \pm\infty$), the two end points of the lines in the Fig. 4 are obtained. Therefore, one could find the value of constant c by using the relation $c = [\delta G(\omega_0 \gg 0) - \delta G(\omega_0 \ll 0)]/2$. We emphasize that this measured stationary-state value for $\langle\tau_3\rangle$ is by no means related to its initial-sate value (i.e., its value before the measurement starts) because the initial-state's information of the qubit is washed out by the detector during the readout process. Nevertheless, the study of stationary-state properties of a qubit could be still desirable in the sense that one can obtain certain knowledges about the qubit-detector coupled system and use them in performing manipulations or measurements on the qubit [19,44–49].

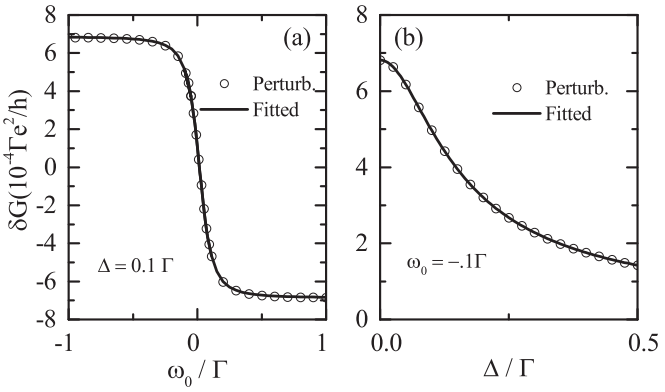

FIG. 6. (a) Plot of δG as a function of ω_0 for $\Delta = 0.1\Gamma$; (b) plot of δG as a function of Δ for $\omega_0 = -0.1\Gamma$. Other parameters are $\varepsilon_d = -1.1\Gamma$, $V_b = 0.5\Gamma$, and $\lambda = 0.01\Gamma$. Circles are perturbative results and solid lines are fittings to the function $f[\omega_0, \Delta]$, with $a = 1.6\times10^{-2}$ and $c = -6.9\times10^{-4}$.

At this point, it is interesting to compare our results for the dependence of δG curves on Δ with the results of Ref. [30]. In that work, it is claimed that the overall shapes of δG would not be altered to the first order in Δ. To show that our results are in accordance at some approximate level with the results of Ref. [30], we could expand the function $\delta G = f[\omega_0, \Delta]$ around small values of Δ; then it is revealed that the correspondence between δG and Δ in Fig. 5(b) is actually provided through next-to-leading order in Δ, i.e., $\delta G_{\Delta\to0} \approx c + \mathcal{O}(\Delta^2)$, which is in accord with the above reference.

IV. CONCLUSIONS

We used the method of nonequilibrium Green's functions to study the effect of electron-electron interaction between a SQD and a singly occupied DQD (charge qubit) on their static and dynamic properties at zero- and finite-bias voltages. To this end, we utilized the infinite-U Lacroix approximation and the Majorana fermion representation of spin operators to find the interacting Green's functions of the system perturbatively to second order in the SQD-qubit coupling constant. We calculated the Green's functions and self-energies of the system in a self-consistent manner with which we could take into account the backaction effects on the system. At zero bias, we checked the accuracy of our results by comparing them with the NRG method. The agreement was good for the density of states of SQD and the expectation value of difference electron occupations of qubit ($\langle\tau_3\rangle$). We found a linear relation between the differential conductance of SQD (δG) and stationary-state expectation value of $\langle\tau_3\rangle$. Concerning with this linear relation, we gave NRG results at zero bias, as a support for our perturbative results, from which perfect linear relation was observed. We also investigated the dependency of δG on various parameters of the system such as V_b, Δ, ω_0, and ε_d. We found that the δG curves are best pronounced at zero-bias voltage and their amplitudes are decreased relatively by increasing bias voltages. Furthermore, we found an approximate functional form for δG with respect to Δ and ω_0. By using this analytical expression, we became able to describe the reason why the authors of Ref. [30] stated that the δG curves are not dependent on the values of Δ.

ACKNOWLEDGMENTS

We acknowledge fruitful discussions with Farshad Ebrahimi. We also thank Amir Eskandari Asl, Babak Zare Rameshti, Micheal Hell, Rok Žitko, and Pablo Cornaglia for their useful comments.

APPENDIX A: EXPRESSIONS FOR SELF-ENERGIES OF SQD AND DQD

In this Appendix, we give the expressions for self-energies of the SQD and the DQD due to the interaction Hamiltonian $\mathcal{H}_I$. The first-order self-energies are identically zero for both the SQD and the DQD because we have taken into account their effect in the noninteracting Green's functions.

The SQD's second-order self-energies are

$$\Sigma_d^{(2nd)R}(\omega) = \lambda^2 \int \frac{d\omega_1}{2\pi}\big[g_d^<(\omega)\Phi^R(\omega-\omega_1) + g_d^R(\omega)\Phi^<(\omega-\omega_1) + g_d^R(\omega)\Phi^R(\omega-\omega_1)\big] \tag{A1a}$$

and

$$\Sigma_d^{(2nd)<}(\omega) = \lambda^2 \int \frac{d\omega_1}{2\pi} g_d^<(\omega)\Phi^<(\omega-\omega_1), \tag{A1b}$$

where

$$\Phi^R(\omega) = \int \frac{d\omega_1}{2\pi}\big[g^<_{\eta,11}(\omega+\omega_1)g^A_{\eta,22}(\omega_1) + g^R_{\eta,11}(\omega+\omega_1)g^<_{\eta,22}(\omega_1) - g^<_{\eta,12}(\omega+\omega_1)g^A_{\eta,21}(\omega_1) - g^R_{\eta,12}(\omega+\omega_1)g^<_{\eta,21}(\omega_1)\big] \tag{A2a}$$

and

$$\Phi^<(\omega) = \int \frac{d\omega_1}{2\pi}[g^<_{\eta,11}(\omega+\omega_1)g^>_{\eta,22}(\omega_1) - {}^<_{\eta,12}(\omega+\omega_1)g^>_{\eta,21}(\omega_1)]. \tag{A2b}$$

For the DQD, the second-order self-energies are

$$\Sigma_\eta^{(2nd)R,<}(\omega) = \begin{pmatrix} F_{22}^{R,<}(\omega) & F_{21}^{R,<}(\omega) & 0 \\ F_{12}^{R,<}(\omega) & F_{11}^{R,<}(\omega) & 0 \\ 0 & 0 & 0 \end{pmatrix}, \tag{A3}$$

where

$$F^R_{mn}(\omega) = \lambda^2 \sum_{\nu=\uparrow,\downarrow} \int \frac{d\omega_1}{2\pi}\big[g^<_{\eta,mn}(\omega)\Pi^R_\nu(\omega-\omega_1) + g^R_{\eta,mn}(\omega)\Pi^<_\nu(\omega-\omega_1) + g^R_{\eta,mn}(\omega)\Pi^R_\nu(\omega-\omega_1)\big] \tag{A4a}$$

and

$$F^<_{mn}(\omega) = \lambda^2 \sum_{\nu=\uparrow,\downarrow} \int \frac{d\omega_1}{2\pi} g^<_{\eta,mn}(\omega)\Pi^<_\nu(\omega-\omega_1). \tag{A4b}$$

In Eqs. (A4), the functions $\Pi_\nu^{R,<}(\omega)$ are given by

$$\Pi_\nu^R(\omega) = \int \frac{d\omega_1}{2\pi}\big[g_{d,\nu\nu}^<(\omega+\omega_1)g_{d,\nu\nu}^A(\omega_1) + g_{d,\nu\nu}^R(\omega+\omega_1)g_{d,\nu\nu}^<(\omega_1)\big] \tag{A5a}$$

and

$$\Pi_\nu^<(\omega) = \int \frac{d\omega_1}{2\pi} g_{d,\nu\nu}^<(\omega+\omega_1)g_{d,\nu\nu}^>(\omega_1). \tag{A5b}$$

APPENDIX B: SELF-CONSISTENT CALCULATIONS

In our numerical results, we have calculated the set of four unknown quantities $[P_\nu(\omega), Q_\nu(\omega), \langle n_{d,\nu}\rangle$, and $\langle\tau_3\rangle]$ by solving self-consistently Eqs. (10), (20), and (21). This way we assure that the backaction effects are correctly taken into account in the results. We used the following scheme.

(i) We start with an initial guess for $\langle n_d\rangle$ and $\langle\tau_3\rangle$ and set $P(\omega) = Q(\omega) = 0$ and then compute $g_d^R(\omega)$ from Eq. (9).

(ii) We calculate $P(\omega)$ and $Q(\omega)$ from computed $g_d^R(\omega)$ and use them to obtain a new $g_d^R(\omega)$. We iterate this step until convergence over $g_d^R(\omega)$ is attained.

(iii) Using the calculated $g_d^{R,<}(\omega)$ and $g_\eta^{R,<}(\omega)$, the self-energies are calculated straightforwardly, and then we use the interacting lesser Green's functions, Eqs. (14) and (19), to calculate new $\langle n_d\rangle$ and $\langle\tau_3\rangle$.

We iterate these three steps until convergence over $\langle n_d\rangle$ and $\langle\tau_3\rangle$ is attained.

APPENDIX C: ANALYTICAL EXPRESSION FOR δG

For a SQD with $U = 0$, it is possible to obtain an analytical expression for the linear relation between δG and $\langle\tau_3\rangle$. To this end, we expand Eq. (23) to the first order in λ, i.e., $\delta G_{\lambda\to 0} \approx \lambda \frac{\partial G_{\lambda\neq 0}}{\partial\lambda}|_{\lambda=0}$, and then, using Eq. (22) and $\mathcal{G}_d^R(\omega) = [\omega - \varepsilon_d - \lambda\langle\tau_3\rangle + i\Gamma - \Sigma_d^{(2nd)R}(\omega)]^{-1}$, we obtain

$$\delta G_{\lambda\to 0} \approx \lambda \sum_{V=\pm\frac{V_b}{2}} \left\{\frac{\Gamma(\varepsilon_d+V)}{\pi[(\varepsilon_d+V)^2+\Gamma^2]^2}\right\}\langle\tau_3\rangle + \mathcal{O}(\lambda^2).$$

One immediate consequence of this expression is that even at the zero-bias voltage there would be an obvious conductance difference in the system; i.e., $\delta G_{V_b=0} \approx \lambda \frac{2\Gamma\varepsilon_d}{\pi(\varepsilon_d^2+\Gamma^2)^2}\langle\tau_3\rangle + \mathcal{O}(\lambda^2)$.

[1] I. L. Aleiner, N. S. Wingreen, and Y. Meir, Dephasing and the Orthogonality Catastrophe in Tunneling Through a Quantum Dot, Phys. Rev. Lett. **79**, 3740 (1997).

[2] S. A. Gurvitz, Measurements with a noninvasive detector and dephasing mechanism, Phys. Rev. B **56**, 15215 (1997).

[3] J. M. Elzerman, R. Hanson, L. H. Willems Van Beveren, B. Witkamp, L. M. K. Vandersypen, and L. P. Kouwenhoven, Single-shot read-out of an individual electron spin in a quantum dot, Nature (London) **430**, 431 (2004).

[4] A. N. Korotkov and D. V. Averin, Continuous weak measurement of quantum coherent oscillations, Phys. Rev. B **64**, 165310 (2001).

[5] H.-S. Goan, G. J. Milburn, H. M. Wiseman, and H. B. Sun, Continuous quantum measurement of two coupled quantum dots using a point contact: A quantum trajectory approach, Phys. Rev. B **63**, 125326 (2001).

[6] T. M. Stace and S. D. Barrett, Continuous Quantum Measurement: Inelastic Tunneling and Lack of Current Oscillations, Phys. Rev. Lett. **92**, 136802 (2004).

[7] H.-A. Engel, V. N. Golovach, D. Loss, L. M. K. Vandersypen, J. M. Elzerman, R. Hanson, and L. P. Kouwenhoven, Measurement Efficiency and n-shot Readout of Spin Qubits, Phys. Rev. Lett. **93**, 106804 (2004).

[8] J. Y. Luo, H. J. Jiao, B. T. Xiong, X.-L. He, and C. Wang, Non-markovian dynamics and noise characteristics in continuous measurement of a solid-state charge qubit, J. Appl. Phys. **114**, 173703 (2013).

[9] R. J. Schoelkopf, P. Wahlgren, A. A. Kozhevnikov, P. Delsing, and D. E. Prober, The radio-frequency single-electron transistor (rf-set): A fast and ultrasensitive electrometer, Science **280**, 1238 (1998).

[10] Y. Nakamura, Y. A. Pashkin, and J. S. Tsai, Coherent control of macroscopic quantum states in a single-cooper-pair box, Nature (London) **398**, 786 (1999).

[11] A. Aassime, G. Johansson, G. Wendin, R. J. Schoelkopf, and P. Delsing, Radio-Frequency Single-Electron Transistor as Readout Device for Qubits: Charge Sensitivity and Backaction, Phys. Rev. Lett. **86**, 3376 (2001).

[12] W. Lu, Z. Ji, L. Pfeiffer, K. W. West, and A. J. Rimberg, Real-time detection of electron tunneling in a quantum dot, Nature (London) **423**, 422 (2003).

[13] O. Astafiev, Y. A. Pashkin, T. Yamamoto, Y. Nakamura, and J. S. Tsai, Single-shot measurement of the josephson charge qubit, Phys. Rev. B **69**, 180507 (2004).

[14] M. D. LaHaye, O. Buu, B. Camarota, and K. C. Schwab, Approaching the quantum limit of a nanomechanical resonator, Science **304**, 74 (2004).

[15] B. A. Turek, K. W. Lehnert, A. Clerk, D. Gunnarsson, K. Bladh, P. Delsing, and R. J. Schoelkopf, Single-electron transistor backaction on the single-electron box, Phys. Rev. B **71**, 193304 (2005).

[16] C. Barthel, M. Kjærgaard, J. Medford, M. Stopa, C. M. Marcus, M. P. Hanson, and A. C. Gossard, Fast sensing of double-dot charge arrangement and spin state with a radio-frequency sensor quantum dot, Phys. Rev. B **81**, 161308 (2010).

[17] A. B. Zorin, F.-J. Ahlers, J. Niemeyer, Th Weimann, H. Wolf, V. A. Krupenin, and S. V. Lotkhov, Background charge noise in metallic single-electron tunneling devices, Phys. Rev. B **53**, 13682 (1996).

[18] A. Grishin, I. V. Yurkevich, and I. V. Lerner, Low-temperature decoherence of qubit coupled to background charges, Phys. Rev. B **72**, 060509 (2005).

[19] Y. Makhlin, G. Schön, and A. Shnirman, Quantum-state engineering with josephson-junction devices, Rev. Mod. Phys. **73**, 357 (2001).

[20] D. Sprinzak, E. Buks, M. Heiblum, and H. Shtrikman, Controlled Dephasing of Electrons *via* a Phase Sensitive Detector, Phys. Rev. Lett. **84**, 5820 (2000).

[21] Y. Makhlin, G. Schön, and A. Shnirman, Statistics and Noise in a Quantum Measurement Process, Phys. Rev. Lett. **85**, 4578 (2000).
[22] A. N. Korotkov, Selective quantum evolution of a qubit state due to continuous measurement, Phys. Rev. B **63**, 115403 (2001).
[23] S. A. Gurvitz and G. P. Berman, Single qubit measurements with an asymmetric single-electron transistor, Phys. Rev. B **72**, 073303 (2005).
[24] S. A. Gurvitz and D. Mozyrsky, Quantum mechanical approach to decoherence and relaxation generated by fluctuating environment, Phys. Rev. B **77**, 075325 (2008).
[25] A. Shnirman and G. Schoen, Quantum measurements performed with a single-electron transistor, Phys. Rev. B **57**, 15400 (1998).
[26] D. Mozyrsky, I. Martin, and M. B. Hastings, Quantum-Limited Sensitivity of Single-Electron-Transistor-Based Displacement Detectors, Phys. Rev. Lett. **92**, 018303 (2004).
[27] N. P. Oxtoby, H. M. Wiseman, and H.-B. Sun, Sensitivity and back action in charge qubit measurements by a strongly coupled single-electron transistor, Phys. Rev. B **74**, 045328 (2006).
[28] C. Emary, Quantum dynamics in nonequilibrium environments, Phys. Rev. A **78**, 032105 (2008).
[29] J. Schulenborg, J. Splettstoesser, M. Governale, and L. D. Contreras-Pulido, Detection of the relaxation rates of an interacting quantum dot by a capacitively coupled sensor dot, Phys. Rev. B **89**, 195305 (2014).
[30] M. Hell, M. R. Wegewijs, and D. P. DiVincenzo, Coherent backaction of quantum dot detectors: Qubit isospin precession, Phys. Rev. B **89**, 195405 (2014).
[31] M. Hell, M. R. Wegewijs, and D. P. DiVincenzo, Qubit quantum-dot sensors: Noise cancellation by coherent backaction, initial slips, and elliptical precession, Phys. Rev. B **93**, 045418 (2016).
[32] A. M. Tsvelik, New Fermionic Description of Quantum Spin Liquid State, Phys. Rev. Lett. **69**, 2142 (1992).
[33] W. Mao, P. Coleman, C. Hooley, and D. Langreth, Spin Dynamics from Majorana Fermions, Phys. Rev. Lett. **91**, 207203 (2003).
[34] A. Shnirman and Y. Makhlin, Spin-Spin Correlators in the Majorana Representation, Phys. Rev. Lett. **91**, 207204 (2003).
[35] C. Lacroix, Density of states for the anderson model, J. Phys. F **11**, 2389 (1981).
[36] R. Bulla, T. A. Costi, and T. Pruschke, Numerical renormalization group method for quantum impurity systems, Rev. Mod. Phys. **80**, 395 (2008).
[37] H.-P. Breuer and F. Petruccione, *The Theory of Open Quantum Systems* (Oxford University Press, New York, USA, 2003).
[38] J. Gorman, D. G. Hasko, and D. A. Williams, Charge-Qubit Operation of an Isolated Double Quantum Dot, Phys. Rev. Lett. **95**, 090502 (2005).
[39] G. Stefanucci and R. van Leeuwen, *Nonequilibrium Many-Body Theory of Quantum Systems: A Modern Introduction* (Cambridge University Press, New York, USA, 2013).
[40] R. Van Roermund, S.-y. Shiau, and M. Lavagna, Anderson model out of equilibrium: Decoherence effects in transport through a quantum dot, Phys. Rev. B **81**, 165115 (2010).
[41] T.-K. Ng, ac Response in the Nonequilibrium Anderson Impurity Model, Phys. Rev. Lett. **76**, 487 (1996).
[42] J. R. Petta, A. C. Johnson, C. M. Marcus, M. P. Hanson, and A. C. Gossard, Manipulation of a Single Charge in a Double Quantum Dot, Phys. Rev. Lett. **93**, 186802 (2004).
[43] R. Žitko, The package is available at http://nrgljubljana.ijs.si.
[44] D. V. Averin, Continuous weak measurement of the macroscopic quantum coherent oscillations of magnetic flux, Phys. C (Amsterdam, Neth.) **352**, 120 (2001).
[45] A. N. Korotkov, Output spectrum of a detector measuring quantum oscillations, Phys. Rev. B **63**, 085312 (2001).
[46] R. Ruskov and A. N. Korotkov, Quantum feedback control of a solid-state qubit, Phys. Rev. B **66**, 041401 (2002).
[47] R. Ruskov and A. N. Korotkov, Spectrum of qubit oscillations from generalized bloch equations, Phys. Rev. B **67**, 075303 (2003).
[48] S. A. Gurvitz, L. Fedichkin, D. Mozyrsky, and G. P. Berman, Relaxation and the Zeno Effect in Qubit Measurements, Phys. Rev. Lett. **91**, 066801 (2003).
[49] T. Gilad and S. A. Gurvitz, Qubit Measurements with a Double-Dot Detector, Phys. Rev. Lett. **97**, 116806 (2006).